Published in the Proceedings of the 16th International Aluminum Alloys Conference (ICAA16) 2018
ISBN: 978-1-926872-41-4
by the Canadian Institute of Mining, Metallurgy & Petroleum

THE EFFECT OF MICROSTRUCTURE ON HOT COMPRESSION DEFORMATION BEHAVIOR OF AN Al-3.8Cu-1.8Li ALLOY

Xiao-Ya Wang[1], Jian-Tang Jiang[1,2], Guo-Ai Li[3] and Liang Zhen[1,*]

[1] *School of Materials Science and Engineering, Harbin Institute of Technology, Harbin 150001, China*
*(*Corresponding author: lzhen@hit.edu.cn)*

[2] *National Key Laboratory of Precision Hot Processing of Metals, Harbin Institute of Technology, Harbin 150001, China*

[3] *Beijing Institute of Aeronautical Materials, Beijing 100095, China*

ABSTRACT

Deformation behavior of 2A97 aluminum alloy containing coarse secondary phases was studied using uniaxial hot compression (HC, 340–490°C, 0.4001–1 s^{-1}). The flow stress could be described by a Zener-Hollomon parameter in hyperbolic sine function with the hot deformation activation energy of 237 kJ/mol. Based on the experimental data and dynamic materials model, processing maps were generated to demonstrate the hot workability of the alloy. The coarse secondary phases experienced dissolution by varying degree under different deformation temperature, which producing different effects on the microstructure evolution. When deformed at relatively low temperatures, a mass of fine grains shaped up in the original grains and grain boundaries, and the dominating deformation mechanism was believed to be dynamic recrystallization. As the deformation temperature rising to 490°C, most secondary phases disappeared and few recrystallized grains were observed, indicating that the secondary phases dissolved sufficiently along with dynamic recovery occurred during the hot deformation. Particle stimulated nucleation related to the coarse secondary phases was believed to promote the recrystallization and the recrystallization behavior was sensitive to deformation temperature.

KEYWORDS

Al-Li alloy, Hot deformation, Particle stimulated nucleation

INTRODUCTION

Al-Li alloys has received much attention as new promising structural materials in the aircraft and aerospace industries, due to their lower density, higher elastic modulus and improved fatigue crack growth resistance in comparison with the conventional commercial aluminum alloys (Ou Ling, 2015). 2A97 alloy is one of the 3rd generation Al-Li alloys targeting at comprehensive improvement of aviation aluminum alloy and applications for wing spars and ribs to other internal structures for transport aircraft. Al-Li alloys are usually formed by hot deformation, either by rolling or extruding. The deformation behavior and resulted microstructure evolution during the forming process mainly dominates the formability of the alloy and the serving performances as well. Therefore, the deformation behavior and microstructure evolution at elevated temperature need be made clear for optimizing the hot processing parameters and controlling microstructure evolution.

Microstructure evolution during the hot deformation is associated with dynamic restoration like dynamic recovery (DRV) and dynamic recrystallization (DRX). DRX is identified as the key restoration process of microstructure evolution during hot working. Specially, it was accepted that DRV is the mechanism which causes aluminum alloys to be softened during hot deformation. This is attributed to the high stacking fault energy that causes easy dislocation climb and cross slip. Many reports have shown that dynamic recrystallization only occurs at low Zener-Hollomon parameters, which must be below or equal to a critical value (Li, Pan, & Yin, 2014; Ruihua Zhu, 2015; Yang et al., 2017).

Secondary phases may strongly affect the microstructure evolution during hot working. A fine dispersion of particles inhibits both grain nucleation and grain boundary migration rates due to Zener pinning pressure; while large particles (>1 μm) may act as sites for particle stimulated nucleation (PSN), which usually results in accelerated recrystallization kinetics, fine grain size and a near random texture (Huang, 2018). PSN has been extensively studied in many materials and much valuable information was provided to help understanding the mechanism and its application (De Siqueira, 2013; Humphreys, 1977, 1979, 2004; Khani Moghanaki, 2017). In Al-Li alloys, PSN is reported to be triggered by large particles containing manganese, iron et al which have a low dispersoid density and heterogeneous distribution, however, the grain refinement and texture modification are not desirable (Khani Moghanaki, 2017)

Limited works on hot deformation behavior and corresponding microstructure evolution of 2A97 alloy are found in open publications so far. The research of the relationship between Z values and the microstructure is very important for industrial production in order to provide evidence for controlling and predicting the structure and performance after hot deformation. In the present study, the deformation behavior and microstructure evolution of 2A97 aluminum alloy containing coarse secondary phases during isothermal compression were studied in detail by building true stress–true strain curves, constitutive equation calculation, processing map and microstructure characterizations, which aimed to reveal the relationship among flow stress and deformation parameters, microstructure evolution and the softening mechanism affected by the secondary phases at different deformation conditions.

EXPERIMENT

The starting material is 2A97 Al-Li alloy with composition of 3.8Cu-1.3Li-0.6Mg-0.6Zn-0.4Mn-0.1Zr and the balance Al (all in weight %). The ingot was two-stage homogenized at 460°C for 6 h and 520°C for 48 h in air furnace and air cooled. Coarse secondary phases with an average size of 10 μm evenly dispersed in the homogenized 2A97 alloy as shown in Figure1a. The secondary phases formed and grew quickly during air cooling process due to the increased driving force as the alloy elements dissolved sufficiently during homogenization. XRD analysis (Figure1b) indicated that the secondary phases were mainly Al_2CuLi (T_1 phase) with dissolution beyond 400°C due to DSC curves in Figure1d.

Cylindrical specimens with a diameter of 8 mm and a height of 12 mm were cut from the homogenized ingot. Isothermal compression were conducted at temperature range of 340–490°C and strain rate range of 0.001–1 s^{-1} on a thermos-mechanical Gleeble-1500D simulator. The specimens were heated at

10°C/s and held for 1 min at the test temperature. Subsequently, the specimens were compressed to a true strain of 0.7 and then quenched into water of about 20°C. In order to reduce the friction, graphite paper was used as lubricant between the crosshead and specimen during hot compression. The compressed specimens were sectioned parallel to the compression axis for microstructure observation.

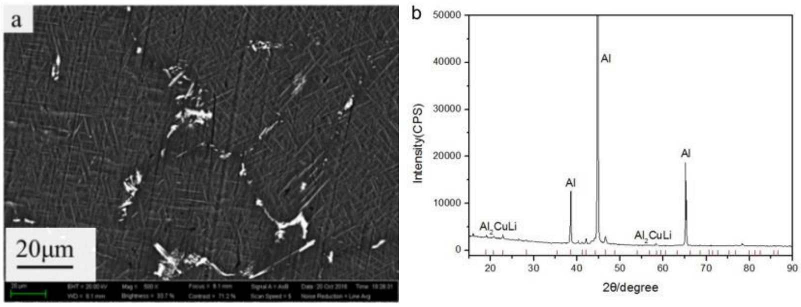

Figure 1. (a) SEM microstructure and (b) XRD pattern of homogenized 2A97 alloy

Scanning electron microscopy (SEM) observation was done using a SUPPA 55 SAPPHIRE SEM equipped with energy-dispersive spectroscopy (EDS). Electron backscattered diffraction (EBSD) analysis was carried out on a SUPPA 55 SAPPHIRE and the data were analyzed using the HKL Channel 5 system. X-ray diffraction characterizations were performed on Rigaku D/max-IIIB X-ray diffraction with a scanning speed of 10°/min and 2θ diffraction angle range of 20–80° and indexed using the 2014 ICDD database. Specimens for EBSD analysis were first mechanically ground and polished, and then electro-polished in a solution of perchloric acid and alcohol with the ratio of 1:9 for 15 s.

RESULTS AND DISCUSSION

Stress-strain Behavior

The flow stress-strain curves of the homogenized 2A97 alloy exhibited typical dynamic softening during compression process as shown in Figure 2. With increasing of the strain, the flow stress increases rapidly up to a peak stress because of rapid dislocation multiplication, and then decreases or keeps stable, which indicating flow softening such as dynamic recovery and recrystallization during the hot compression deformation. The flow stress of the alloy varied under different deformation conditions. When deformation temperature kept unchanged, the flow stress increased with increasing strain rate, indicating the higher efficiency of restoration processes during deformation processes. This is because there is no sufficient time for energy accumulation and dislocation annihilation at higher strain rate.

Specially, the alloy was sensitive to positive temperature. When deformed at low temperature (340–460°C), the stress-strain curves exhibited single peak stress at initial deformation stage, followed by the flow stress keeping decreasing. It represented typical deformation softening characteristic resulting from DRX (Eddahbi, 1998). The softening produced by continuous DRX contributed to the drop of the flow stress. When deformed at 490°C, the flow curves presented multiple peak stress which was the typical characteristic of DRV. Dynamic softening including recovery and recrystallization is important process responsible for the microstructure evolution during high temperature deformation. Generally, during the deformation of high stacking fault energy metal, DRV occurred at lower deformation temperature and higher strain rate while the softening mechanism changed into DRX at higher deformation temperature and lower strain rate. In the present work, however, the softening behavior of the experiment alloy presented different characteristic. This must be ascribed to the effects of the coarse secondary phases in the homogenized alloy.

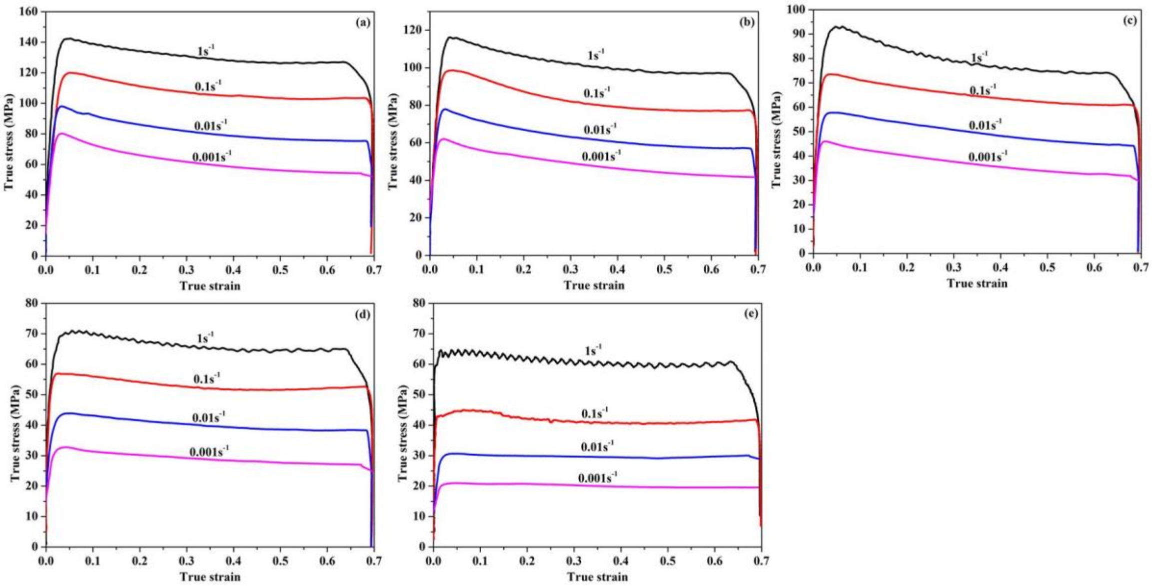

Figure 2. Stress-strain curves at different temperatures and strain rates of homogenized 2A97 alloy

Kinetic Analysis

In the isothermal compression of aluminum alloy materials at high temperature, it is well accepted that the relationship between flow stress, strain rate and temperature can be expressed as (Zener, 1944; Cerri, 1997)

$$\mathrm{Z} = A_1\sigma^{n_1} \tag{1}$$

$$\mathrm{Z} = A_2 exp(\beta\sigma) \tag{2}$$

Where A_1,A_2,n_1 and β are constants; Z is the Zener-Hollomon parameter; Q is the activation energy; R is the gas constant. In addition, the hyperbolic sine type equation, Eq.(3) is more general in form suitable for stress over a wide range, especially for expressing the hot deformation behavior of aluminum alloy(Sellars, 1966; Meng Gang, 2009; Medina, 1996):

$$\mathrm{Z} = A(sinh\alpha\sigma)^n \tag{3}$$

Where A and n are constants； α is the stress multiplier and it is calculated as $\alpha=\beta/n_1$,where β is taken as the average values of slopes of $\ln\acute{\varepsilon}$ vs. σ plots at low stress, n_1 is taken as the average values of the slopes of $\ln\acute{\varepsilon}$ vs. $\ln\sigma$ at high stress. Constitutive equation Eq. (4) can be obtained from Eq. (1) to Eq. (3):

$$\dot{\varepsilon} = A_3[sinh(\alpha\sigma)^n]\left(-\frac{Q}{RT}\right) \tag{4}$$

In order to investigate the hot deformation behavior, four unknown parameters Q, A, α and n should be calculated. Differentiating Eq. (4) gives,

$$\mathrm{Q} = \mathrm{R}\left|\frac{\partial ln\dot{\varepsilon}}{\partial ln[sinh(\alpha\sigma)]}\right|_T \left|\frac{\partial ln[sinh(\alpha\sigma)]}{\partial(1/T)}\right|_{\dot{\varepsilon}} \tag{5}$$

In the present study, the peak flow stress σ_p was analyzed using the hyperbolic sine equation.

Figures 3(a-e) showed the relationships between strain rate and flow stress from which the Zener-Hollomon parameters in the hyperbolic sine equation of the homogenized 2A97 alloy were calculated and shown in Eq. (6).

$$\dot{\varepsilon} = 1.36 \times 10^{23}[sinh(0.017)]^{5.37} exp\left(-\frac{237598}{RT}\right) \tag{6}$$

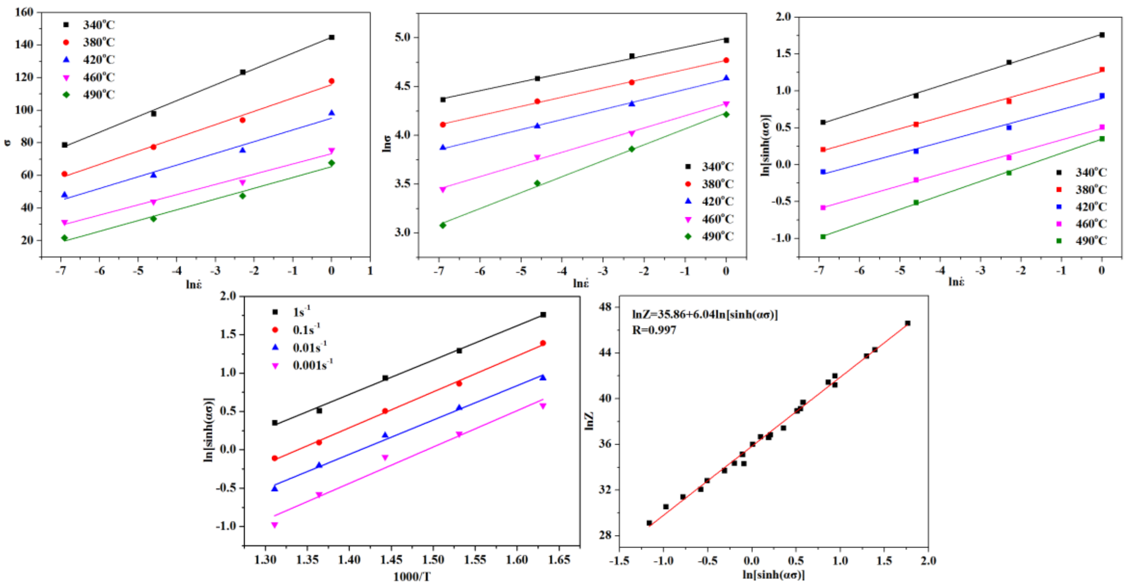

Figure 3. Relationship between strain rate and flow stress: (a) σ-ln$\dot{\varepsilon}$; (b) lnσ-ln$\dot{\varepsilon}$; (c) ln[sinh(ασ)]-ln$\dot{\varepsilon}$; (d) ln[sinh(ασ)]-1000/T; (e) lnZ- ln[sinh(ασ)]

The hot deformation activation energy is an important physical parameter serving as an indicator of deformation difficulty degree in plastic deformation. In the present work, the Q value of the experiment alloy was 237 kJ/mol, which was consistent with the compression activation energy of other homogenized Al-Li alloys with deformation mechanism of dynamic recrystallization couple with dynamic recovery (Li et al., 2014; Yang et al., 2017). The value of Q was found to be about 282 kJ/mol for the 8090 alloy (McQueen, 1996) and 303.14 kJ/mol for 1460 alloy (Xiang et al., 2015). The existent fine secondary phases precipitated during deformation process of these alloys, which hindered the movement of dislocations and made the dynamic recovery more difficult.

Processing Map

Based on dynamic material modeling (DMM), the processing map has been established recently by Prasad et al., which is widely used to study the deformation behavior of many materials (Lin, 2013; Liu Wenyi, 2014; Prasad, 1998). In this model, the work piece subjects to hot deformation are assumed to dissipate power. The instantaneous power dissipated (P) may be separated into two complementary parts, i.e., G content and J co-content. G represents the power dissipated by plastic work while J is the energy dissipated by dynamic microstructural changes. Therefore the total dissipated power can be written as follows:

$$\mathrm{P} = \mathrm{J} + \mathrm{G} = \sigma\dot{\varepsilon} = \int_0^{\sigma} \dot{\varepsilon} d\sigma + \int_0^{\dot{\varepsilon}} \sigma d\dot{\varepsilon} \tag{7}$$

At a constant temperature and strain, the dynamic response of the work piece material undergoing hot deformation is represented by the constitutive equation:

$$\sigma = \mathrm{K}\dot{\varepsilon}^{m} \tag{8}$$

The strain rate sensitivity (m) of flow stress is used to partition power between G and J, since

$$\mathrm{m} = \frac{dJ}{dG} = \frac{\dot{\varepsilon} d\sigma}{\sigma d\dot{\varepsilon}} = \frac{\varepsilon\sigma \dot{d} ln\sigma}{\sigma \dot{\varepsilon} ln\dot{\varepsilon}} \approx \frac{\Delta log\sigma}{\Delta log\dot{\varepsilon}} \tag{9}$$

From Eqs. (8)–(9), J is described as follows:

$$\mathrm{J} = \sigma\dot{\varepsilon}m/(m+1) \tag{10}$$

For an ideal linear dissipater, m=1 and $J=J_{max}$. The efficiency of power dissipation of a non-linear dissipater may be expressed as a dimensionless parameter:

$$\eta = \frac{J}{J_{max}} = \frac{2m}{m+1} \tag{11}$$

The variation of efficiency with temperature and strain rate constitutes a power dissipation map. The extremum principles of irreversible thermodynamics are applied to continuum mechanics of large plastic flow as described by Prasad (1990) develop a continuum criterion combining these principles with those of separability of power dissipation and have shown that flow instability will occur during hot deformation:

$$\xi(\dot{\varepsilon}) = \frac{\partial ln\left(\frac{m}{m+1}\right)}{\partial(ln\dot{\varepsilon})} + m < 0 \tag{12}$$

The negative ζ value means forging or rolling processing under the experimental temperature and strain rate is "unsafe" with manifestations of adiabatic shear bands, flow localizations, dynamic strain aging, flow rotations, et al. The processing maps of the homogenized 2A97 alloy at strain of 0.2, 0.4 and 0.6 are shown in Figure 4. The contours represent the efficiency of power dissipation marked as percent, and shadow domains represent the instability domains. It can be found that the shapes of the processing maps are similar at strains of 0.2, 0.4 and 0.6, and the shade areas (unsafe domains) increase with the increase of strain. The optimum processing parameters are in the strain rate range of around 0.003–0.01 s^{-1} and deformation temperature range between 340 and 490°C with power efficiency of around 23–32%.

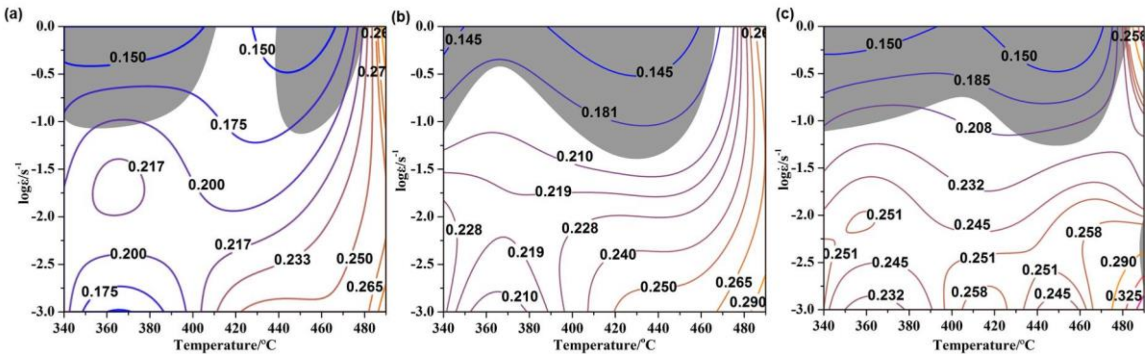

Figure 4. Processing map of homogenized 2A97 under different strain: (a)0.2; (b) 0.4;(c) 0.6

Microstructure Evolution

The coarse T_1 phases with an initial average size of 10 μm experienced fragmentation and dissolution during the hot deformation and the dissolution quantity increased with increasing deformation temperature as shown in Figure 5. Noticeably, T_1 phases presented significant dissolution and the average size reduced to 0.6 μm as the deformation temperature rising to 490°C. Non-deformable second phase particles can have different effects on the recrystallization behavior, mainly depending on their size

(Mandal, 1997). Generally, particles are divided into two distinct categories based on the particle size: coarse particles of size typically >1 μm and fine dispersoids of size ~10–300 nm (Humphreys, 2004). These two classes of particles have strong effects on the recrystallization behavior, with the coarser ones accelerating recrystallization through PSN and the finer ones retarding or even suppressing recrystallization. However, fine particles were found to accelerate recrystallization even though their sizes are smaller than the critical size for PSN. It has been shown using Al–Cu alloys with the same solute content of Cu but with different unstable θ phase (Al_2Cu) particles, that dispersed particles (<0.8 μm) can lead to either acceleration or retardation of recrystallization (Doherty, 1962, 1963). Actually, the critical size of PSN is reported to be related to inter-particle spacing, volume fraction of particles, strain et al. The critical size of T_1 phases in Al-Li alloy will be discussed in our future study. Specially, the secondary phases with different size under different deformation conditions were expected to present different effect on the microstructure evolution of the homogenized 2A97 alloy.

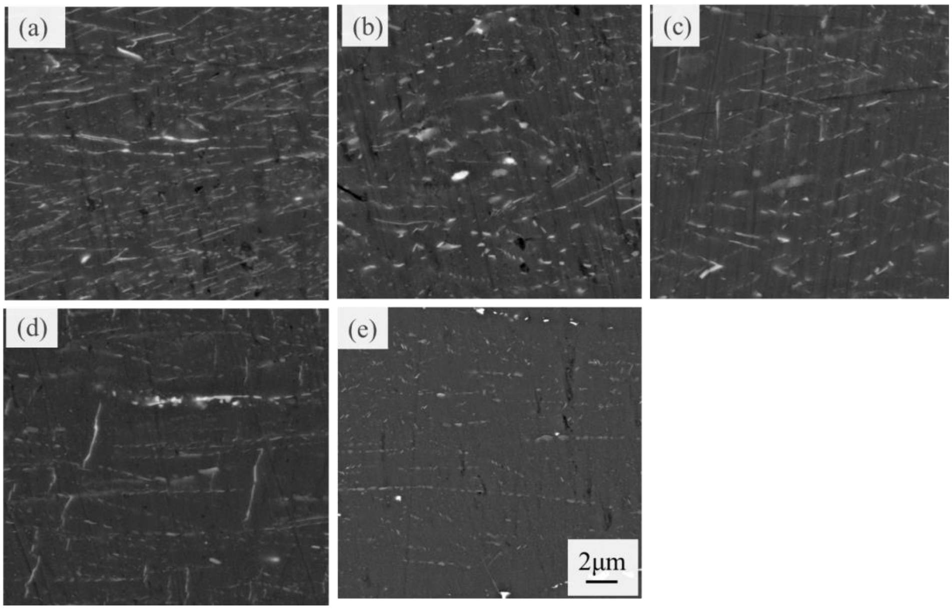

Figure 5. BSE images of the compressed alloy under 0.01 s^{-1} and different deformation temperature showing the fragmentation and dissolution of the coarse secondary phases

Figure 6 represented IPF and grain boundary maps and MAD histograms of specimens deformed at different temperature with the same strain rate. It was obvious that a number of fine new grains nucleated and grew both in the original grain boundaries and inside the original grains when deformed at 340°C as shown in Figure 7a. The fine grains mainly had <001> orientation and random orientation. The fraction of high angle misorientation (HAGB, θ>15°) was 41.9%. These features suggested a DRX microstructure for the specimen deformed at 340°C. The fraction of HAGB reached maximum value of 51.84% at deformation temperature of 380°C, followed by slight decreasing with deformation temperature increasing to 460°C. In addition, the average size of the new grains kept growing up with increasing deformation temperature and reached 6.13 μm at deformation temperature of 460°C. However, grains were found to be elongated along the maximum shear stress direction. The MAD histogram (Figure 6i) exhibited a large fraction of LAGBs. A strong <101> texture, which was typical for face centered cubic (FCC) metals after uniaxial compression deformation, was observed in IPF map (Figure 6d) of the specimen deformed at 490°C. Both the microstructure and misorientation distribution features confirmed that the restoration mechanism for this specimen was DRV.

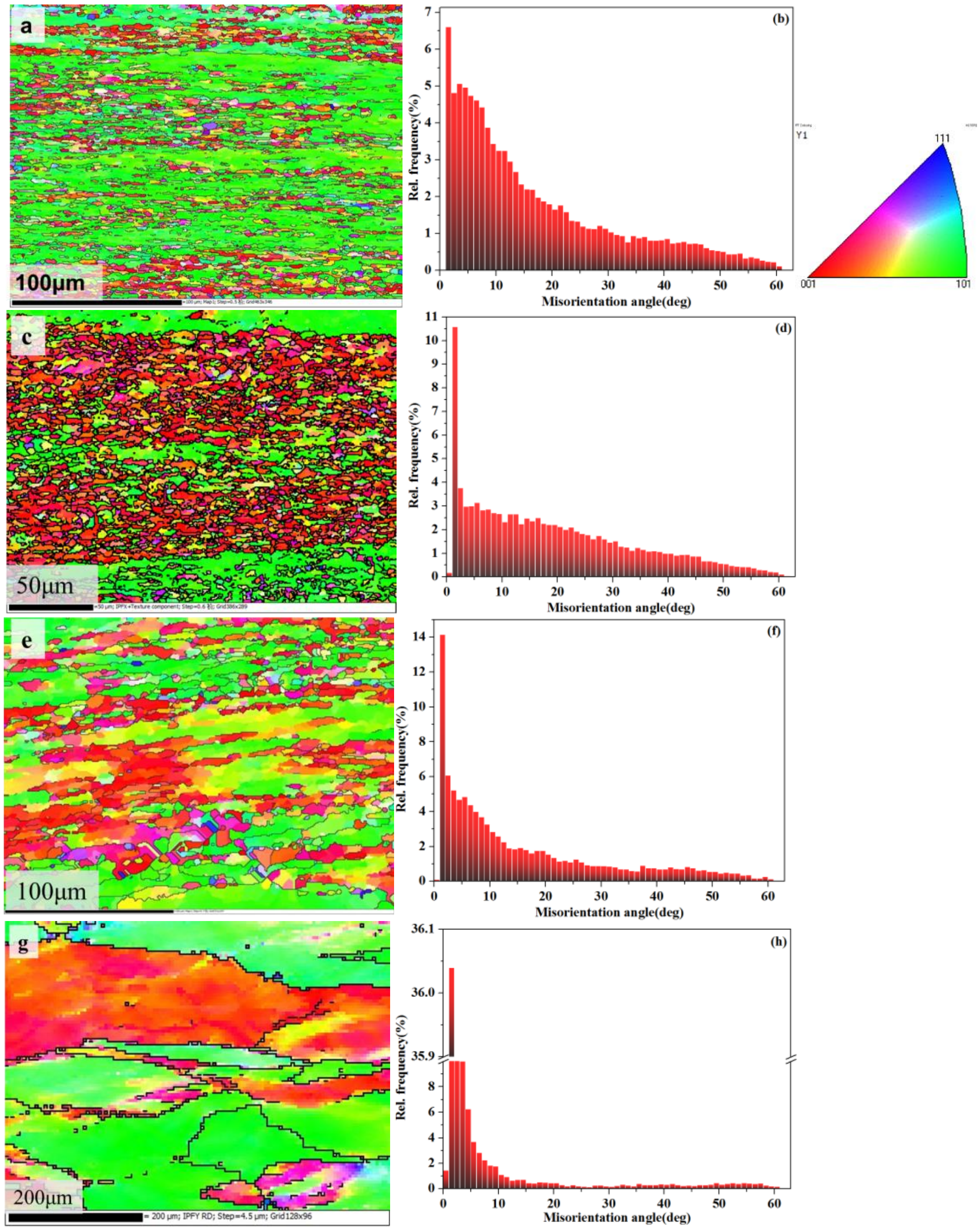

Figure 6. EBSD analysis of specimens deformed at strain rate of 0.01 s^{-1} and different temperatures: (a, b) 340°C; (c, d) 380°C; (e, f) 460°C; (g, h) 490°C

When deformed at 340–460°C, the evolution of microstructure was highly affected by the coarse secondary phases, and dynamic recrystallization was accelerated due to the lattice rotation in the local formation zones adjacent to the particles. Meanwhile, the secondary phases affect the kinetics of grain growth, lead to a limiting grain size and may induce abnormal grain growth. When the deformation temperature increased from 340 to 380°C, the DRX was promoted as the deformation stored energy increased. With the increase of deformation temperature, however, the dissolution of the coarse secondary phases was accelerated leading to decrease of the volume fraction of particles larger than critical size. The acceleration of recrystallization or grain refinement was smaller and the fraction of the new grains lowered with the increase of deformation temperature. Moreover, the higher deformation temperature raised the driving force for the DRX grains growing up.

CONCLUSIONS

Deformation behavior of homogenized 2A97 Al-Li alloy with micro-sized T_1 phases was studied using uniaxial hot compression (HC, 340–490°C, 0.001–1 s^{-1}). Controlled microstructure can be obtained by modifying the deformation conditions. Conclusions obtained from the present work are drawn:

(1) With the increase of temperature and decrease of strain rate, the stress decreases significantly. Constitutive equation based on the hyperbolic sine equation is established and the apparent activation energy of hot compression is estimated to be 237 kJ/mol.

(2) The processing maps are similar in the strain ranging from 0.2-0.6 and the unsafe domains increases with the increase of strain. The optimum hot-working condition of 2A97 alloy is 340–490°C and 0.001–0.03 s^{-1}.

(3) The coarse T_1 phases experience fragment and dissolution during hot deformation, and the dissolution quantity increased observably with the increase of deformation temperature, which exerts different effects on the microstructure evolution of the homogenized 2A97 alloy. Specially, the size of the secondary phases is lower than the critical size of PSN when deformed at 490°C.

(4) Dynamic recrystallization is the main soften mechanism due to particles stimulation nucleation and fine grains are obtained at deformation temperature of 340–460°C. When deformed at 490°C, the soften mechanism changes to dynamic recovery.

REFERENCES

C. Zener, J. H. H. (1944). Effect of Strain rate upon plastic flow of steel. *Journal of Applied Physics, 15*, 22–27.

C.M. Sellars, W. J. T. (1966). The relationship between the resistance and the structural deformation in the hot, Memories Scientific Review. *Acta Metall., 63*, 731–746.

D Mandal, I. B. (1997). On the effect of fine second-phase particles on primary recrystallization as a function of strain. *Acta Materialia, 45*(2), 453–461. doi:10.1016/S1359-6454(96)00215-7

De Siqueira RP, S. H., Raabe D. . (2013). Particle stimulated nucleation in coarse-grained ferritic stainless steel. *Metall Mater Trans A, 44*, 469–478.

E Cerri, E. E., A Forcellese, HJ Mcqueen. (1997). Comparative hot workability of 7012 and 7075 alloys after different pretreatments. *Materials Science and Engineering: A, 197*(2), 181–198.

Huang, K. M., Knut Zhao, Qinglong Logé, Roland E. (2018). The double-edge effect of second-phase particles on the recrystallization behaviour and associated mechanical properties of metallic materials. *Progress in Materials Science, 92*, 284–359. doi:10.1016/j.pmatsci.2017.10.004

Humphreys, F. J. (1977). The nucleation of recrystallization at second phase particles in deformed aluminium *Acta matall., 25*, 1323–1344.

Humphreys, F. J. (1979). Local lattice rotations at second phase particles in deformed metals *Acta matall., 27*, 1801–1824.

Humphreys, F. J. (2004). Nucleation in Recrystallization. *Materials Science Forum, 467–470*, 107–116. doi:10.4028/www.scientific.net/MSF.467-470.107

Humphreys FJ, H. M. (2004). *Recrystallization and related annealing phenomena. 2nd ed*: Elsevier.

Khani Moghanaki, S. K., Mohsen Logé, Roland. (2017). Recrystallization behavior of multi-directionally forged over-aged and solution treated Al-Cu-Mg alloy during non-isothermal annealing. *Materials & Design, 132*, 250–256. doi:10.1016/j.matdes.2017.07.011

Li, B., Pan, Q., & Yin, Z. (2014). Characterization of hot deformation behavior of as-homogenized Al–Cu–Li–Sc–Zr alloy using processing maps. *Materials Science and Engineering: A, 614*, 199–206. doi:10.1016/j.msea.2014.07.031

Lin Y, C. L., Lei-Ting. Xia, Yu-Chi Jiang, Yu-Qiang. (2013). Hot deformation and processing map of a typical Al–Zn–Mg–Cu alloy. *Journal of Alloys and Compounds, 550*, 438–445. doi:10.1016/j.jallcom.2012.10.114

Liu Wenyi, Z. H., Li Dan, Zhang Zhiqing, Huang Guangjie, Liu Qing. (2014). Hot deformation behavior of AA7085 aluminum alloy during isothermal compression at elevated temperature. *Materials Science and Engineering: A, 596*, 176–182. doi:10.1016/j.msea.2013.12.012

M. Eddahbi, F. C. o. a. O. A. R. (1998). Microstructural Changes During High Temperature Deformation of an Al-Li(8090) Alloy. *Scripta Materialia, 38*(11), 1717–1723.

McQueen, G. A.-C. D. P. J. (1996). Hot deformation mechanisms of a solution-treated Al-Li-Cu-Mg-Zr alloy. *Metallurgical and Materials Transactions A, 27*(11), 3478–3490.

Meng Gang, L. B., Li Hongmei, Huang Hui, Nie Zuoren. (2009). Hot deformation and processing maps of an Al–5.7wt.%Mg alloy with erbium. *Materials Science and Engineering: A, 517*(1–2), 132–137. doi:10.1016/j.msea.2009.03.068

Ou Ling, Z. Z., Nie Yufeng, Jian Haigen. (2015). Hot deformation behavior of 2060 alloy. *Journal of Alloys and Compounds, 648*, 681–689. doi:10.1016/j.jallcom.2015.07.027

Prasad, Y. (1990). Processing maps for hot working of 47Zr–45Ti–5Al–3V alloy. *Indian Journal of Science and Technology, 28*, 435–451.

RD Doherty, J. M. (1962-1963). The effect of a dispersed second phase on the recrystallization of aluminum-copper alloys. *J. Inst. Metals, 91*(91), 332–339.

Ruihua Zhu, Q. L., Jinfeng Li, Sheng Xiang, Yonglai Chen, Xuhu Zhang. (2015). Dynamic restoration mechanism and physically based constitutive model of 2050 Al-Li alloy during hot compression. *Journal of Alloys and Compounds, 650*, 75–85. doi:10.1016/j.jallcom.2015.07.182

S.F. Medina, C. A. H. (1996). General expression of the Zener-Hollomon parameter as a function of the chemical composition of low alloy and microalloyed steels. *Acta Materialia, 44*(1), 137–148.

Saeed Khani Moghanaki, M. K. a. R. L. (2017). Recrystallization behavior of multi-directionally forged over-aged and solution treated Al-Cu-Mg alloy during non-isothermal annealing. *Materials & Design, 132*, 250–256. doi:10.1016/j.matdes.2017.07.011

Xiang, S., Liu, D.-y., Zhu, R.-h., Li, J.-f., Chen, Y.-l., & Zhang, X.-h. (2015). Hot deformation behavior and microstructure evolution of 1460 Al–Li alloy. *Transactions of Nonferrous Metals Society of China, 25*(12), 3855–3864. doi:10.1016/s1003-6326(15)64033-x

Y.V.R.K. Prasad, T. S. (1998). Processing maps for hot working of titanium alloys. *Materials Science and Engineering: A, 243*(1–2), 82–88.

Yang, Q., Wang, X., Li, X., Deng, Z., Jia, Z., Zhang, Z., . . . Liu, Q. (2017). Hot deformation behavior and microstructure of AA2195 alloy under plane strain compression. *Materials Characterization, 131*, 500–507. doi:10.1016/j.matchar.2017.06.001